

# Dynamics of the Self-Propelled Motion of a Polymer Solvent Droplet

Abraham Reddy

Advisor: Alexander Wagner

North Dakota State University  
SPS Final Report

May 10, 2007

## 1 Introduction

In this project I investigate the dynamics of the self-propelled motion of a polymer solvent droplet. Similar movement has been witnessed in a variety of situations. For example oil placed on glass substrate coated with Stearyl Trimethyl Ammonium ions exhibits this motion due to the chemical Marangoni effect. Here the droplet absorbs the hydrophobic molecules on the substrate leaving an absence of them behind and an excess in front creating the difference in surface tension[1]. This has also been witnessed during the melting of solid layers of alkenes into droplets. The droplets then move across the surface in a self avoiding path consuming the solid alkene, leaving behind a widening groove[2]. Though there are similarities between these and our situation, current research has not been done to explain the dynamics of this polymer solvent situation. This motion is produced when a droplet of polymer solvent is placed on the surface of the non-solvent bath. This phenomenon was discovered experimentally by Marshall Bremer in the spring of 2006 while attempting to create circular polymer membranes. He performed multiple experiments to determine the cause of this motion. He looked at the action of the solvent when placed on the surface, finding that it quickly spread across the surface but just as quickly disappeared possibly by diffusion or evaporation. He also investigated the dilution of the non-solvent with solvent, finding that this cause the droplet to slow and become more sporadic. From these experiments he speculated that the movement of the droplet was most likely caused by the spreading of the layer of solvent underneath the droplet to areas which have a lower density of the solvent. I want to investigate the motion of this droplet in a fluid dynamic simulation using the lattice Boltzmann algorithm. I hope to determine the mechanism by which these droplets the motion of the droplets is driven[3].

## 2 Experimental Observations

This observed phenomenon of self-propelled motion was observed and characterized in the spring of 2006 by Marshall Bremer. Marshall was studying polymeric membranes formed by immersion precipitation. The process used to create them involves spreading a thin layer of solvent-polymer solution onto a substrate, usually glass. The substrate is then dipped into a non-solvent. The solvent mixes with the non-solvent, while the polymer forms a thin porous membrane. The formation of the pores is believed to be the result of a phase transition. This transition occurs as the solvent leaves the polymer and is replaced by non-solvent. The repulsion of these two components causes the polymer and non-solvent to separate. As the polymer chains condense, they become entangled and prevent the completion of the phase transition. The pores are created as a result of this[3, 4].

The movement was initially witnessed when an attempt was made to create a small circular polymer membrane. When placing the polymer solvent on the surface of a non-solvent bath, the droplet would move rapidly across the surface, with such movement lasting up to twelve minutes. After this observation, he performed several experiments to investigate the cause of the motion.

Using a non-solvent consisting of pure de-ionized water, the motion was found to be continuous with a top speed of approximately 0.2 m/s. After diluting the non-solvent with solvent to a level of 17 percent DMF, the motion became slower and more sporadic. The droplet would move a few centimeters and after a few seconds, it would again move off in a random direction. While studying the motion closely, there appeared to be a jet of solvent protruding out from one side of the droplet pushing it in the opposite direction. There also appeared to be a region of solvent located on the underside of the droplets. It was considered that this region could possibly be contacting the non-solvent surface on one side of the droplet causing the solvent to spread and hence creating the appearance of a solvent jet. The effect of the DMF on the surface was also tested. A needle damp with DMF was dipped in the non-solvent near a droplet that had completed formation. This caused an immediate movement of the droplet of a few centimeters. This process was also immediately repeatable. It was decided that the mechanism could have the ability to produce the motion.

The action of the DMF was also investigated. To do this, small particles were placed on the surface. The solvent was then dripped on the surface causing the particles to quickly spread. However, the surface would quickly return to normal. Similar effects were observed with acetone solvent. It was conjectured that the recovery of the surface could possibly be due to the diffusion and/or the evaporation of the solvent[3].

Observations of the movement were then conducted again, this time using the surface covered with particles. The movement of the polymer droplet created a tear shaped wake which was void of particles. The droplet also prevented particles from collecting on its leading edge which was surmised to be from the spreading of small amounts of solvent from that side. It was finally concluded that the spreading of the solvent was most likely the mechanism for the motion.



**Fig. 1** From left to right: 1) Initial configuration of surface at time 0.0s. 2) Effect of solvent drop on surface at time = 0.4s. 3) Recovery of surface at time = 1.5s[3].



**Fig. 2** Photograph of droplet of PVDF-solvent solution moving over surface littered with small particles. Droplet is curving left and is located near the bottom left of the open space. You can see the small wake left behind the droplet. This wake will quickly be replaced with particles as the droplet moves on[3].

### 3 Model

We wish to numerically model this situation to determine the mechanism by which the droplet moved. To do this we start by modeling the spreading of the solvent on the surface. As observed experimentally the solvent quickly spread across the surface of the non-solvent, but eventually seems to disappear. We will model this by creating a two component model of the solvent and the non-solvent where the solvent has an affinity for the surface. General equations of motion (assumed isothermal) for the two components, the convection-diffusion equation for each component as well as the navier-stokes equation for the total fluid, are given below

$$\partial_t \rho_A + \nabla(\rho_A u) = \nabla \left( k \frac{\rho_A \rho_B}{\rho} (\nabla \mu_A - \nabla \mu_B) \right) \quad (1)$$

$$\partial_t \rho_B + \nabla(\rho_B u) = \nabla(k \frac{\rho_A \rho_B}{\rho} (\nabla \mu_B - \nabla \mu_A)) \quad (2)$$

$$\partial_t(\rho u) + \nabla(\rho u u) = -\rho_a \nabla \mu_A - \rho_B \nabla \mu_B + \nabla \sigma \quad (3)$$

where  $\rho_A$  and  $\rho_B$  are the densities of the non-solvent and solvent respectively,  $\rho$  is the total density,  $\sigma$  is the Newtonian stress tensor and  $\mu_A$  and  $\mu_B$  are given by

$$\mu_A = \frac{\delta F}{\delta \rho_A} \quad (4)$$

$$\mu_B = \frac{\delta F}{\delta \rho_B} \quad (5)$$

To include this affinity we will apply a constant force on the solvent near the surface. This is incorporated into the free energy which is given by

$$F = \int \theta \rho_A \log\left(\frac{\rho_A}{1 - b\rho}\right) + \theta \rho_B \log\left(\frac{\rho_B}{1 - b\rho}\right) + \rho_B V(y) \quad (6)$$

where  $V(y)$  is the linear surface potential which will be applied in the first two lattice rows and  $b$  is the excluded volume parameter from the Van der Waals equation of state.

Since the effect of solvent quickly disappears from the surface we will also let it diffuse into the bulk. The solvent, which is initially concentrated at a point, wishes to spread and diffuse into the bulk, but the affinity for the surface keep it from completely diffusing. This should induce a circular flow field below the surface of the non-solvent. Now we need to look at the action of the droplet on a layer of solvent. As concluded experimentally the jets from the solvent under the droplet were probably caused by the desire of the solvent to spread to areas which contain lower densities of itself. To model this we will convert some of the B densities to A densities which will spread according to our equations of motion. For the boundary conditions, we will model the liquid-gas interface as a slip boundary and the bottom as a non-slip boundary. The side boundaries will be periodic. To implement this model we will employ the lattice Boltzmann algorithm.

## 4 Lattice Boltzmann

The lattice Boltzmann equation is a discretization of the Boltzmann equation using the BGK approximation expressed below

$$f_i(r + v_i \Delta t, t + \Delta t) - f_i(r, t) = \Delta t \left( \frac{1}{\tau} (f_i^e(r, t) - f_i(r, t)) + F_i \right) \quad (7)$$

Here  $r$  is the position on the lattice,  $v$  is the velocity of the particle,  $\tau$  is the relaxation time parameter, and  $F$  and  $G$  are non-ideal forcing terms. In order to implement this we need to define an equilibrium distribution that corresponds

to the velocity moments of the equilibrium distribution function. For the two dimensional implementation of this using 9 velocity vectors at each lattice point, known as the D2Q9 model the equilibrium distribution is given by

$$f_i^0 = nw_i \left[ 1 + \frac{3}{c^2} u_\alpha v_{i\alpha} + \frac{9}{2c^4} (u_\alpha v_{i\alpha})^2 - \frac{3}{2c^2} u_\alpha u_\alpha \right]. \quad (8)$$

where the  $w_i$  are given by[5]

$$\begin{aligned} w_0 &= 4/9 \\ w_{1,2,3,4} &= 1/9 \\ w_{5,6,7,8} &= 1/36 \end{aligned} \quad (9)$$

and the moments for the forcing terms are given by[5]

$$\sum_i F_i = 0 \quad (10)$$

$$\sum_i F_i v_{i\alpha} = -nF_\alpha \quad (11)$$

$$\sum_i F_i v_{i\alpha} v_{i\beta} = -n(F_\alpha u_\beta + u_\alpha F_\beta) \quad (12)$$

$$\sum_i F_i v_{i\alpha} v_{i\beta} v_{i\gamma} = -n[F_\alpha(\theta\delta_{\beta\gamma} + u_\beta u_\gamma) + F_\beta(\theta\delta_{\alpha\gamma} + u_\alpha u_\gamma) \quad (13)$$

$$+ F_\gamma(\theta\delta_{\alpha\beta} + u_\alpha u_\beta)]. \quad (14)$$

## 4.1 Multicomponent Systems

To simulate a multicomponent system using lattice Boltzmann we must first compare it to the implementation of a single component system. For a multicomponent system the Navier-Stokes equation and the continuity equation are valid for the total fluid density but since the momentum of each component is not conserved separately there is no Navier-Stokes equation for each component. Instead, the dynamics of the individual components are governed by a convection diffusion equation. For multiple components we first look at the lattice Boltzmann equation for this given by

$$f_i^\sigma(r + v_i \Delta t, t + \Delta t) - f_i^\sigma(r, t) = \Delta t \left( \frac{1}{\tau} (f_i^{\sigma e}(r, t) - f_i^\sigma(r, t) + G_i^\sigma) + F_i^\sigma \right) \quad (15)$$

where  $\sigma$  indicates an individual component. The moments of the equilibrium distribution are defined in an analogous fashion. Summing over Eq.(15) we recover the lattice Boltzmann equation of the overall density given by Eq.(7). Using the same procedure we can recover the continuity equation and Navier-Stokes equation in the same form as the single component system. By Taylor

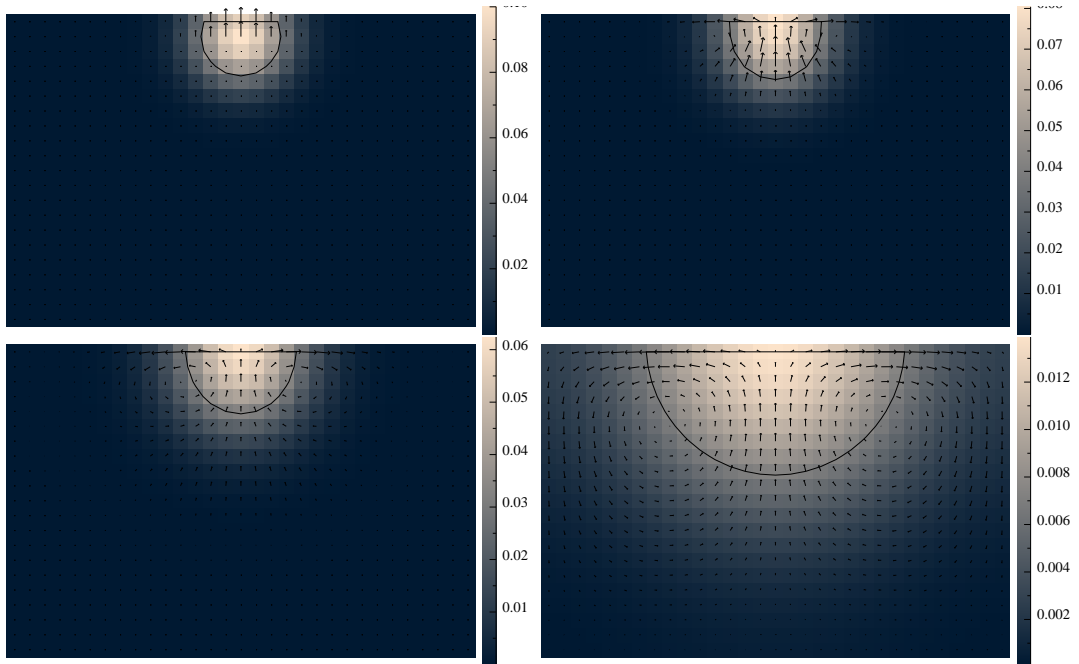


**Fig. 3** From left to right and top to bottom: a) Initial density and velocity vectors. b) Material begins spreading across surface. c) Circular flow field begins to be induced. d) Induced circular flow field.

expansion we can also recover the convection diffusion equations for each components. Now, however, the macroscopic physical quantities are that of the overall system[6]. From these equations we can now simulate a multicomponent system.

## 5 Progress

### 5.1 Initial Results

I am implementing a two dimensional two component lattice Boltzmann algorithm. To do this I started by making a two component model in which we will simulate the chemical potential by making one of the components prefer the boundary. We will call them A particles and B particles. To apply this preference I implemented a density dependent force on the B particles acting within the top two rows of the lattice. The simulation implements periodic boundaries on the sides as well as slip boundaries on the top and non-slip boundaries on the bottom. Initially, we have produced the action of the spreading of the solvent. The solvent moves out from its highest density point while also slightly diffusing into the bulk creating the expected circular flow field beneath the surface.

## 5.2 Spreading of the Solvent

After observing that the expected flow pattern was induced using the addition of a surface potential in the free energy, I continued by creating a model for the oozing of the solvent from underneath the polymer droplet that was seen experimentally. I did this by creating a zone in which A densities were converted to B densities according to a conversion factor. This kept the overall density of the system constant. The position of this zone is determined by its midpoint and its radius. From this the full and partial lattice spaces overlapped by the zone are calculated. Then the densities at each of these lattice spaces are converted from A to B according to the percentage of the space overlapped by the conversion zone and a variable conversion factor.

## 5.3 Movement of the Particle

The polymer particle was created similarly to the way the solvent was. The size and position of the particle is also specified by its midpoint and radius. It also has a given mass  $m$ . To see if movement could be induced, we needed to transfer momentum from the fluid to the particle. To do this, the full and partial lattice spaces overlapped by the zone are once again calculated. In these regions we transfer the x momentum of the fluid to the particle according to a factor which control the efficiency of the transfer. We then adjust the momentum of the fluid according the the amount transfered to the particle. The velocity and distance moved by the particle is then calculated from the transfered momentum. The midpoint of the oozing zone is also updated according to the movement of the particle.

The first case we considered was the symmetric situation where the midpoint of the solvent oozing zone and the particle zone coincide. For this situation there was no movement witnessed as shown in Figure 4. Also, as show in Figure \* even when given an initial velocity the particle quickly stops.

We then considered the asymmetric case where the midpoint of the particle zone is offset from the midpoint of the solvent zone by a given amount of lattice spaces,  $dx$ . In this case we see that some movement is induced. As shown in Figure 5 the particle quickly accelerates to a speed of approximately  $3.25 * 10^7$  then slowly loses speed. We also see from Figure 6 that for different  $dx$  we find the maximum velocity of the particle varies with the amount of offset. We also see from this that there is an optimum offset.

## 5.4 Exploring the Parameter Space

In our system we have four free parameters, the van der Waals excluded volume parameter  $b$ , the relaxation time parameter, the conversion factor of A to B particles, and the surface potential forcing. Initially  $b$  was zero and the latter three parameters were investigated. Now that we have seen that movement can be induced, we would like to find out for which values of these parameters our system will behave most like the physical situation. To investigate this we will

Velocity vs Time of Symmetric Situation

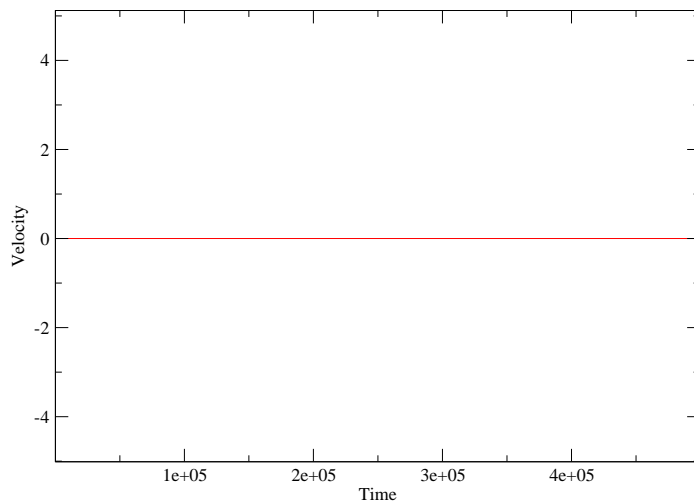


**Fig. 4** The velocity of the particle vs. time for the case where the midpoint of the solvent oozing zone and the particle zone coincide.

look at the maximum value of velocity in our system as well as the average velocity squared once it reaches equilibrium. This was done over a range of the values for each parameter while the other parameters were held constant. From this we can determine the most advantageous values for our parameters. To do this we first determined the number of iterations it would take for the system to reach equilibrium by looking at the velocities of the system in time. Using this I then varied the parameter as described before.

The first parameter investigated was the conversion rate. From Figure 7 we see that both the max velocity as well as average velocity squared increased linearly with the conversion rate. Which was as expected because a larger conversion rate would cause larger velocities; and since we are modeling an ideal gas at this point the densities aren't limited, so we wouldn't expect the velocity to plateau.

Next, the relaxation time parameter, which determines the viscosity via  $\nu = \theta(\tau - 1/2)$ , was varied. A graph of this is given in Figure 8. Here the the max velocity and average velocity squared decreased as  $\frac{1}{\nu^2}$ . This seems reasonable because at lower viscosity a higher velocity would be expected. Also, as viscosity increases, it makes sense the velocity should decrease asymptotically toward zero because it would become harder and harder for the fluid to flow.

Finally, the surface potential forcing was investigated. Here we see some unusual behavior. This is most noticeable in the kink at the end of the graph

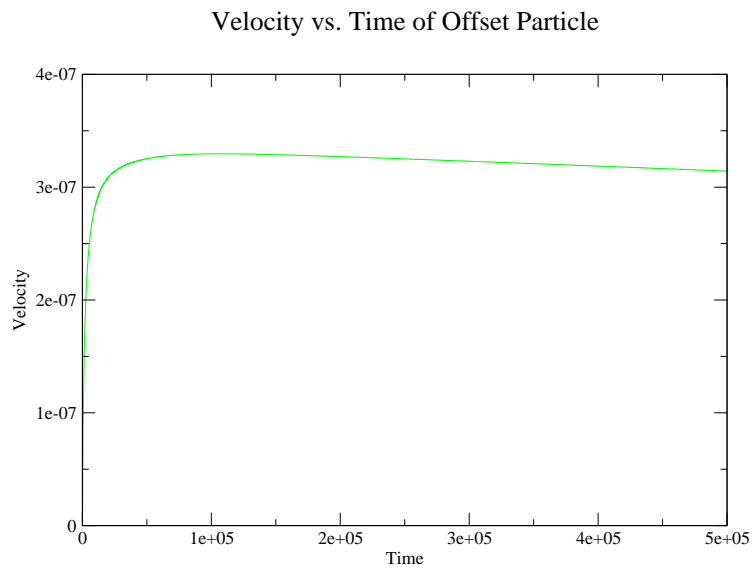


**Fig. 5** The velocity of the particle vs. time for the case where the midpoint of the solvent oozing zone and the particle zone are offset by a fraction of the radius,  $dx$ . The surface forcing is  $F = 10^{-3}$ .

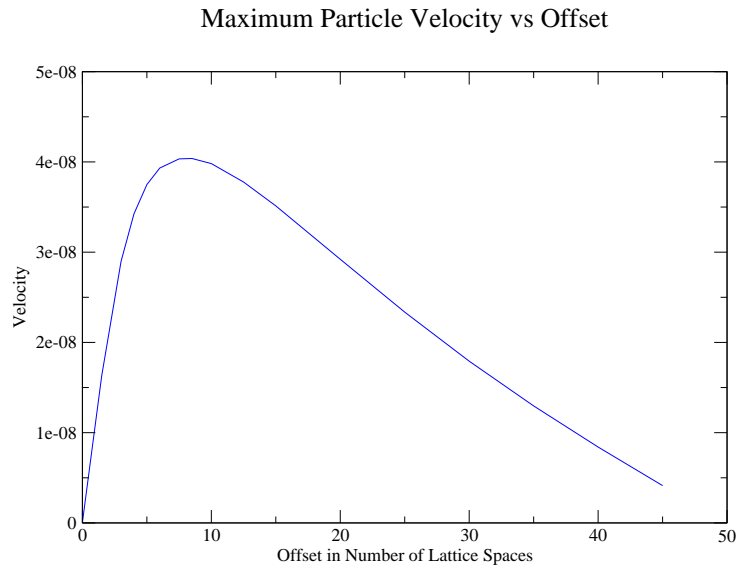


**Fig. 6** Maximum velocity vs. Offset. Parameters: couple = .1; mass = 2;  $1/\tau$ ;  $F=10^{-5}$ ; conversion factor =  $10^{-4}$

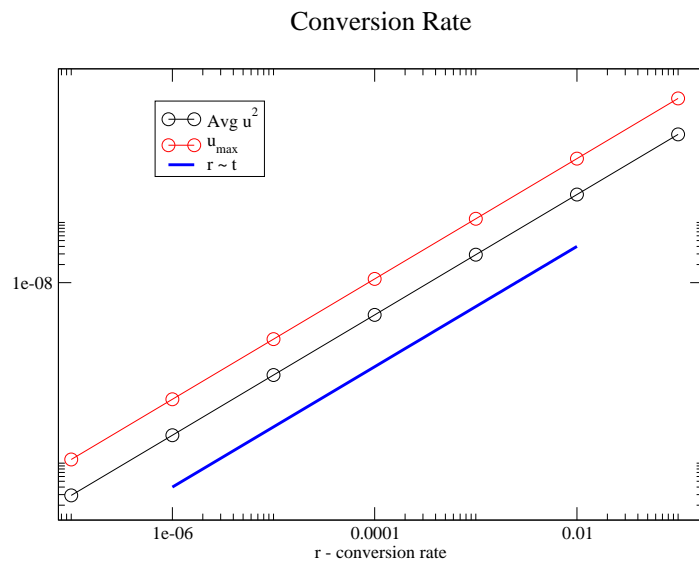


**Fig. 7** Velocity and average velocity square for varied conversion rates.

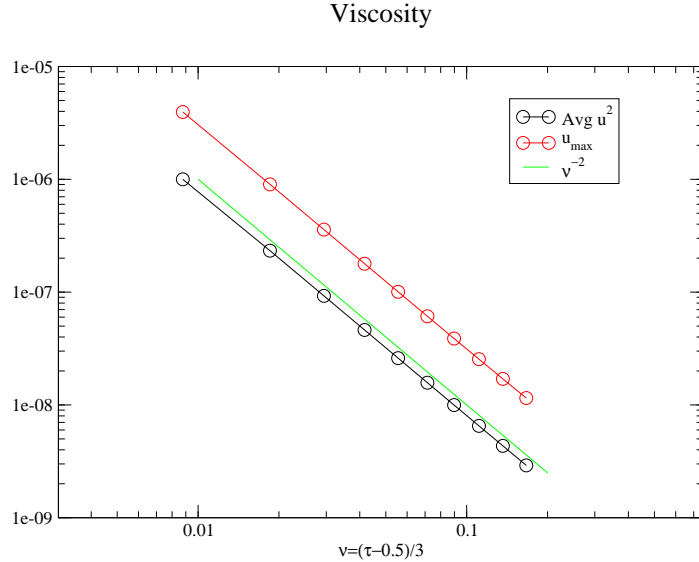


**Fig. 8** Velocity and average velocity squared for varied viscosity.

in Figure 9.

For the largest forcing, it seemed as if the system might not have reached a stationary state. To test this I increased the number of iterations for each parameter value. This is shown in Figure 10.

Surprisingly, this had the opposite effect from what I had expected. The max velocity and average velocity squared were now farther from the fitted relationship. To find out what was happening we again looked at the system over time, this time for different values of the forcing.

From this, the problem was readily apparent. As show in Figure 11 the system was not actually reaching a stationary state. For lower forces the curve is much more gradual, so it had appeared as if it had reached a stationary state when it hadn't.

## 5.5 The Chemical Potential

In equilibrium the chemical potential a system should become a constant. In our case, however, it was not. It was this gradient in the chemical potential that needed to be fixed to make our system physical. At higher forces, B particles were becoming trapped near the surface causing the densities in this region to become large. The occurrence of these large density was allowed in the ideal gas model we were using. In this model, the particles have no volume, so the densities can become infinitely large. To deal with this problem moved from the ideal gas to the Van der Waals equation of state.

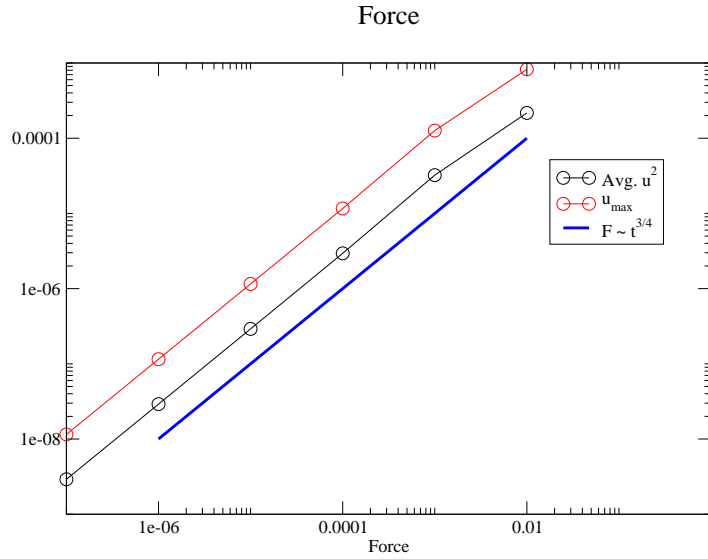


**Fig. 9** Velocity and average velocity squared for varied surface forcing.

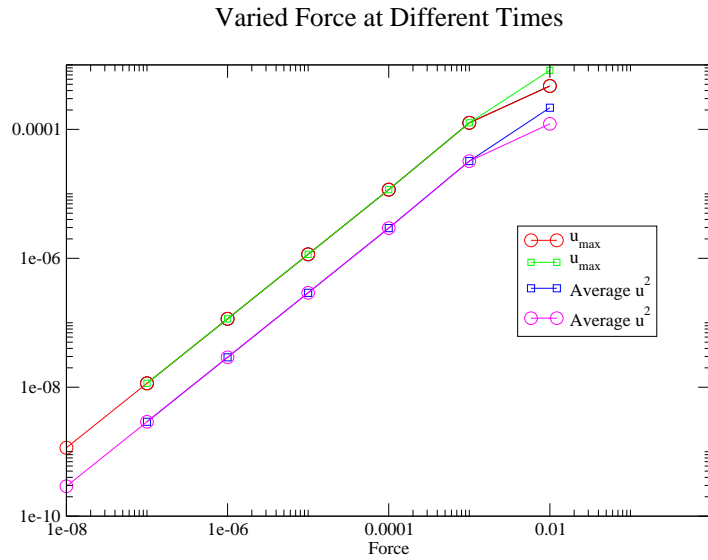


**Fig. 10** Velocity and average velocity squared vs. varied surface forcing for the same starting parameters run for different lengths of time. Red and Purple were run 500000 iterations. Green and Blue were run 300000 iterations.

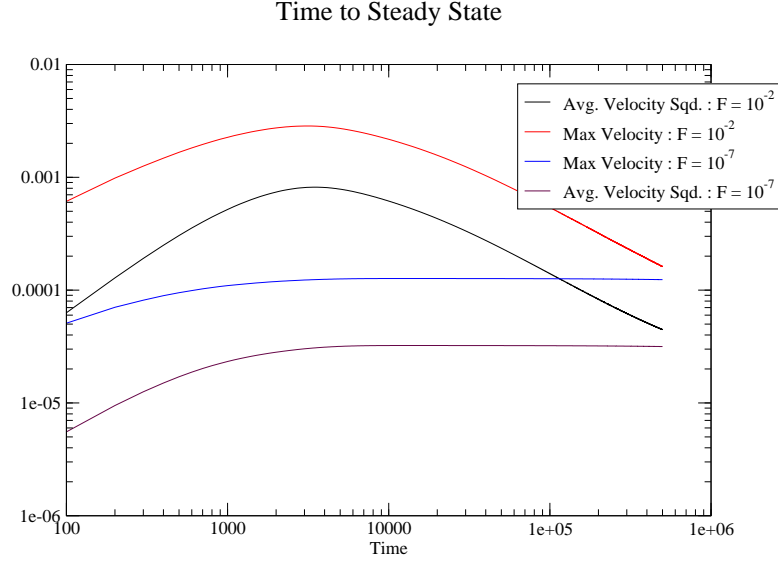


**Fig. 11** Velocity and average velocity squared vs. time for  $F = 10^{-7}$  and  $F = 10^{-2}$ .

### 5.5.1 Van der Waals Equation of State

The Van der Waals equation of state is given by

$$(V - b) \left( P + \frac{a}{V^2} \right) = NkT \quad (16)$$

where  $a$  is related to the attraction of the particle and  $b$  is related to the excluded volume. From this we see that the pressure is given by

$$P = \frac{nkT}{1 - nb/N} - \frac{an^2}{N^2} \quad (17)$$

We are only concerned here with the volume of the particle and not the interaction so we can set  $a = 0$ . In our case we have two components, so we must find the Van der Waals equation of state for each component. Doing so we have

$$P_A = \frac{n_A kT}{1 - nb/N} \quad (18)$$

$$P_B = \frac{n_B kT}{1 - nb/N} \quad (19)$$

where  $n_A$  and  $n_B$  are the densities of each component. To implement this we see that our pressure is related to our forcing by

$$nF_\alpha = -\partial_\beta (P_{\alpha\beta} - n\theta\delta_{\alpha\beta}). \quad (20)$$

Using this along with the discrete gradient approximation given by

$$\partial_x P = \frac{1}{2}(P[x + 1] - P[x - 1]) \quad (21)$$

we can include this in our forcing[5]. Additionally we are able to write our forcing in terms of  $\mu$ . Doing so we see that our forcing can be given by

$$-F_\alpha = n_\alpha \nabla \mu_\alpha - \frac{\theta n_\alpha}{3} \quad (22)$$

Including the Van der Waals equation of state greatly improved the gradient in our chemical potential did not succeed in creating a constant chemical potential at equilibrium.

### 5.5.2 Higher Order Corrections

To achieve a chemical constant potential we need to include additional higher order corrections when calculating our forcing. The method we use is derived in Wagner et al[7]. There, a constant chemical potential is achieved up to machine accuracy for a one dimensional model. Since the gradient in our chemical potential is only in the y direction we have a one dimensional problem for which this method will work. To do this we add the correction, given by

$$\tau \Psi = \left(\tau - \frac{1}{4}\right) \frac{FF}{\rho} + \frac{1}{12} \nabla^2 \rho \quad (23)$$

to the second moment of the forcing[7].

After the addition of the correction, no improvement in the gradient of the chemical potential was found. This was most likely due to an incorrect implementation of the forcing. We then calculated the forcing by using the chemical potential  $\mu$  given in Eq. (22), rather than the pressure. This was the method used by Wagner[7]. Still no improvement in the chemical potential was found.

## 6 Conclusion

Our model of the system was shown to induce motion. The size of this motion was very small and varied depending on our free parameters. However, the gradient found in the chemical potential limits the validity of our results. The results given in this paper concerning the movement of the particle were with a smaller surface potential, so the gradient in the chemical potential was less apparent. From the results so far we can not say if this motion is the main cause of the the movement witnessed by Marshall Bremer. To do this we would need to normalize our system so that our times and distances were in terms of meters and seconds rather than lattice spaces and iterations.

After numerous attempts to correct the error in the chemical potential no improvement was made besides the original addition of the Van der Waals forcing. Reworking of my code would probably be needed to correct this.

## References

- [1] Y. Sumino, N. Magome, T. Hamada, and K. Yoshikawa, *Self-Running Droplet: Emergence of Regular Motion from Nonequilibrium Noise*, Phys. Rev. Lett. **94**, 868301 (2005).
- [2] P. Lazar and H. Riegler, *Reversible Self-Propelled Droplet Movement: A New Driving Mechanism*, Phys. Rev. Lett. **95**, 136103 (2005)
- [3] M. Bremer and A. Jones, *Solvent Propulsion of Polymeric Membranes on Non-solvent Surface*, Interim report for SPS grant, Spring 2006.
- [4] J. F. Hester, P. Banerjee, and A. M. Mayes, *Preparation of Protein-Resistant Surfaces on Poly(vinylidene fluoride) Membranes via Surface Segregation*, Macromolecules **1999**, 32, 1643-1650.
- [5] A.J. Wagner, *Thermodynamic consistency of liquid-gas lattice Boltzmann simulations*, arXiv:cond-mat/0607087v2.
- [6] Q. Li, *Theory of the Lattice Boltzmann Method for Multi-phase and Multi-component Fluids*, M.S. thesis, North Dakota State University, Fargo ND, May 2007
- [7] A. J. Wagner, *A Practical Introduction to the Lattice Boltzmann Method*, Adt. notes for Statistical Mechanics 463/663 at NDSU.